



Neuromodulation with transcutaneous spinal stimulation reveals different groups of motor profiles during robot-guided stepping in humans with incomplete spinal cord injury

Matthias J. Krenn^{1,2,3} · Jason M. White^{4,5} · Dobrivoje S. Stokic² · Keith E. Tansey^{1,2,6}

Received: 16 August 2022 / Accepted: 3 December 2022
© The Author(s), under exclusive licence to Springer-Verlag GmbH Germany, part of Springer Nature 2022

Abstract

Neuromodulation via spinal stimulation has been investigated for improving motor function and reducing spasticity after spinal cord injury (SCI) in humans. Despite the reported heterogeneity of outcomes, few investigations have attempted to discern commonalities among individual responses to neuromodulation, especially the impact of stimulation frequencies. Here, we examined how exposure to continuous lumbosacral transcutaneous spinal stimulation (TSS) across a range of frequencies affects robotic torques and EMG patterns during stepping in a robotic gait orthosis on a motorized treadmill. We studied nine chronic motor-incomplete SCI individuals (8/1 AIS-C/D, 8 men) during robot-guided stepping with body-weight support without and with TSS applied at random frequencies between 1 and up to 100 Hz at a constant, individually selected stimulation intensity below the common motor threshold for posterior root reflexes. The hip and knee robotic torques needed to maintain the predefined stepping trajectory and EMG in eight bilateral leg muscles were recorded. We calculated the standardized mean difference between the stimulation conditions grouped into frequency bins and the no stimulation condition to determine changes in the normalized torques and the average EMG envelopes. We found heterogeneous changes in robotic torques across individuals. Agglomerative clustering of robotic torques identified four groups wherein the patterns of changes differed in magnitude and direction depending mainly on the stimulation frequency and stance/swing phase. On one end of the spectrum, the changes in robotic torques were greater with increasing stimulation frequencies (four participants), which coincided with a decrease in EMG, mainly due to the reduction of clonogenic motor output in the lower leg muscles. On the other end, we found an inverted u-shape change in torque over the mid-frequency range along with an increase in EMG, reflecting the augmentation of gait-related physiological (two participants) or pathophysiological (one participant) output. We conclude that TSS during robot-guided stepping reveals different frequency-dependent motor profiles among individuals with chronic motor incomplete SCI. This suggests the need for a better understanding and characterization of motor control profiles in SCI when applying TSS as a therapeutic intervention for improving gait.

Keywords Spinal cord injury · Neuromodulation · Electrical stimulation · Motor control · Locomotion · Robotic gait orthosis

Introduction

Spinal cord injury (SCI) affects the interactions between supraspinal structures and the spinal cord neural networks below the injury. It results in partial or complete loss of volitional control of movements (e.g., standing, stepping,

etc.). The ensuing muscle weakness is often accompanied by spastic motor states, such as increased muscle tone (hypertonia), hyperactive reflexes (hyperreflexia), pathological reflexes (clonus), as well as involuntary muscle contractions (spasms), and improper muscle coordination (dyssynergia) (Adams and Hicks 2005; Dietz and Sinkjaer 2007).

Current rehabilitation strategies to improve walking after SCI are based on the principles of neural recovery through task-specific training (Smith and Knikou 2016; Harvey 2016; Musselman et al. 2018). Manual-assisted (Wernig et al. 1999; Beres-Jones and Harkema 2004; Domingo et al. 2007) or robot-assisted (Hornby et al. 2005; Wirz et al. 2005;

Communicated by Winston D Byblow.

Matthias J. Krenn
mkrenn@umc.edu

Extended author information available on the last page of the article

Winchester et al. 2005, 2009; Hayes et al. 2018) treadmill training provides an environment in which highly stereotyped and repetitive rhythmic sensory input from receptors in the trunk and lower limbs is synchronized with the stepping cycle to generate or augment gait-related motor output. These sensory inputs may engage local circuitry in the spinal cord (Jankowska 2017) and supraspinal centers (Winchester et al. 2005) in incomplete injury to promote gait recovery. However, the efficacy of intense treadmill locomotor training after SCI depends on injury severity (Côté et al. 2017), with improvements documented mainly in people with motor incomplete SCI (Hubli and Dietz 2013; Dietz and Fouad 2014).

New developments in electrical neuromodulation with epidural (ESS) or transcutaneous (TSS) spinal stimulation show promise for improving walking after SCI. The underlying premise of ESS and TSS interventions is that the generated afferent input modifies the excitability of the lumbosacral network to either augment appropriate or suppress pathophysiological spinal motor output (Mayr et al. 2016; James et al. 2018). Furthermore, anecdotal reports in humans suggest that the spinal cord isolated from supraspinal influence has the ability to transform continuous afferent input provided by spinal stimulation into rhythmic motor output (Dimitrijevic et al. 1998). Studies in SCI individuals had reported improvements in postural and stepping functions when continuous ESS was applied in combination with intense locomotor training (Angeli et al. 2014, 2018; Grahn et al. 2017; Calvert et al. 2019) but also without formal training (Darrow et al. 2019). In recent years, TSS has emerged as a non-invasive alternative to ESS and, at lower cost and surgical risk, may permit the study of more individuals economically and safely. The accumulated evidence suggests that TSS is feasible for enhancing motor function after SCI (Megía García et al. 2020; Estes et al. 2021). TSS has been applied to assist with sit-to-stand transfer and support standing (Sayenko et al. 2019; Al'joboori et al. 2020). Providing 30-min of TSS at the beginning of 2 h gait and mobility exercises showed improvements in different walking metrics across the group of 10 motor incomplete SCI persons (McHugh et al. 2020). Notably, several studies reported that TSS can immediately modify muscle activation patterns during treadmill stepping in clinically motor complete (Minassian et al. 2016; Zaaya et al. 2021) and incomplete SCI (Hofstoetter et al. 2015; Gerasimenko et al. 2015b; Meyer et al. 2020), or in combination with other interventions (Murray and Knikou 2019; Pulverenti et al. 2021; Zaaya et al. 2021).

Although the existing studies provide insights into the potential of ESS and TSS to improve different aspects of motor control in people with SCI, the knowledge about their effects on gait kinematics and muscle activation patterns is limited. In addition, no criteria were established to identify an adequate candidate for a specific type of neuromodulation

intervention (Hofer and Schwab 2019). One reason for this lack of specificity of neuromodulation is that in nearly all previous studies, the results were analyzed on a group level without sufficient attention to quantifying likely diverse individual physiological profiles and stimulation response characteristics. Understanding this diversity is expected to guide the development of individually tailored stimulation interventions.

Moreover, the selection of stimulation parameters seems critical for diverse applications of ESS and TSS neuromodulation interventions; however, currently, there is no agreed-upon approach or well-defined criteria by which to choose these parameters. With ESS, multiple stimulation parameters (electrode pad selection, stimulation intensity, and frequency) have been adjusted in some combinations iteratively and individually to arrive at the best possible parameters for achieving the desired goals (Angeli et al. 2014, 2018; Cuellar et al. 2017; Gill et al. 2018; Darrow et al. 2019). Some groups (Gerasimenko et al. 2008; Minassian et al. 2012; Hofstoetter et al. 2018) have proposed the use of specific ranges of frequencies for different purposes: 5–15 Hz to support upright standing, around 30–50 Hz to augment stepping, and 50–100 Hz to reduce lower-limb spasticity. As a result, the previously mentioned TSS studies have adopted these recommendations and examined only limited stimulation frequencies.

To address the impact of a broader range of TSS frequencies on locomotion and to investigate the possible spectrum of responses in people with motor incomplete SCI, we took an alternative approach and allowed stimulation frequencies to vary randomly from 1 up to 100 Hz during robot-guided stepping. In this experimental environment, we examined the robotic torques necessary to keep the hip and knee joints on a predefined stepping trajectory and the associated electromyographic (EMG) signals from the main lower limb muscles in motor incomplete SCI participants. We anticipated individually specific patterns of robotic torque and EMG modulation that may be associated with different stimulation frequency ranges and aimed to determine commonalities and differences across individuals.

Material and methods

Participants

Nine participants (Table 1) with motor incomplete traumatic SCI (ASIA Impairment Scale C or D) were recruited. The inclusion criteria were > 6 months post-injury, preserved patellar and Achilles tendon reflexes, no active implants at the site of stimulation, ability to safely sustain an upright position and bear some body weight in the robotic exoskeleton as assessed by the study physical therapists, meeting

Table 1 Demographic and injury data of the participants with stimulation and robotic settings

ID	Sex	Age (years)	TSI (years)	AIS	NLI	LEMS	BWS (%)	CMT (mA)	Stim. intensity (mA)	Frequency range (Hz)	Number of tested frequencies
S1	M	57.1	3.5	C	T10	3	50	160	110	1–100	29
S2	M	32.1	5.0	C	C6	0*	60	120	90	1–100	46
S3	M	41.5	4.1	C	C5	15	40	110	75	1–100	28
S4	M	49.5	1.9	D	C5	N/A	40	140	86	1–50	39
S5	M	40.6	1.6	C	T3	N/A	60	75	40	1–100	29
S6	M	18.1	1.5	C	C6	7	60	100	22	1–100	29
S7	M	51.5	0.8	C	C7	15	40	130	80	1–50	37
S8	M	21.1	0.6	C	T1	9	40	65	45	1–60	28
S9	F	21.3	1.1	C	T3	6	50	70	50	1–100	46

Clinical records contemporary to the time of the study were used. In two records, the NLI and AIS were recorded but the data collection sheets containing LEMS scores were not available at the time of data analysis

TSI time since injury, AIS ASIA impairment scale, NLI neurological level of injury, C cervical, T thoracic, LEMS lower extremity motor score, BWS body-weight support during the study, CMT common motor threshold for eliciting posterior root reflexes in all muscles during rest in weight-supported standing, * voluntary movement in non-key muscles, N/A not available

the criteria for height (1.5–2.0 m) and weight (< 135 kg) for the robotic exoskeleton, and no contraindications for robot-assisted stepping (unstable blood pressure, bone instability, open wounds, circulatory problems, cardiac contraindications, significant leg length discrepancy, hip, knee or ankle joint injury/disease or significant limitations in the range of motion, or pregnancy). Written informed consent was obtained as approved by the local Institutional Review Board.

Study procedures

The procedures used here were similar to a previous study conducted at the same institution in clinically complete SCI (Minassian et al. 2016). The participants were first instrumented with EMG recording and TSS stimulation electrodes (see below) in supine. Then, the participants were placed in the body-weight support harness and fitted into the robotic gait orthosis (Lokomat Pro, Hocoma AG, Volketswil, CH), as is customary for clinical purposes and recommended by the manufacturer. The Lokomat was used in a research mode, which provided real-time analog data output of robotic torques and angles (Fig. 1a).

Robot-guided treadmill stepping

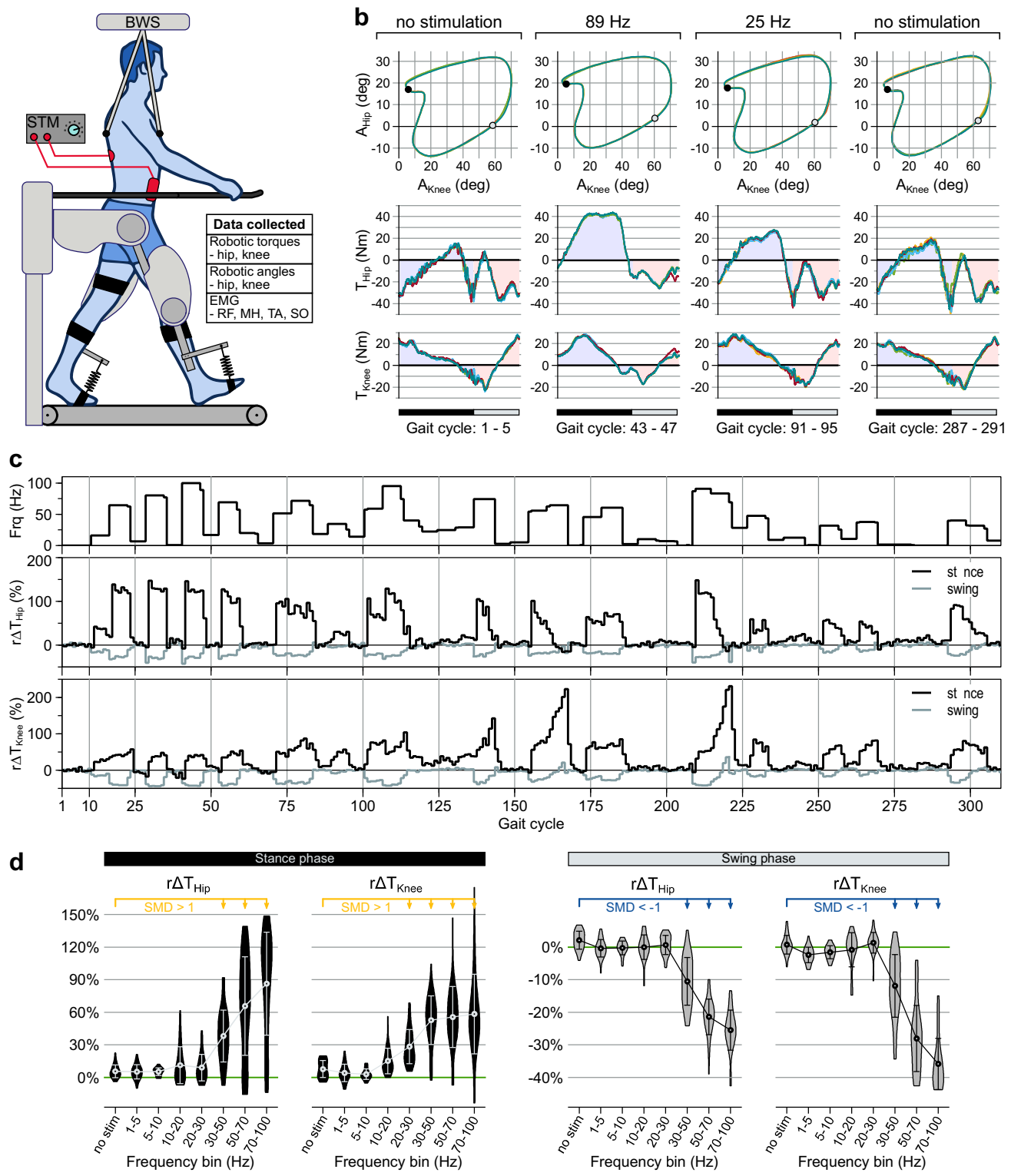
Body-weight support was set to the minimum necessary to allow safe, comfortable, and continued walking without leg buckling (40–60% of the body weight, Table 1) at a treadmill speed of 0.56 m/s (2 km/h). The Lokomat consists of an actively driven gait orthosis that controls the hip and knee angles in the sagittal plane during the

gait cycle. For this, the hip and knee joints are actuated as needed by linear drives integrated into the orthosis. The two orthotic joints follow predefined trajectories (Riener et al. 2005, 2006) using a position control strategy (Jezernik et al. 2003). Some degree of deviation between the actual and pre-set trajectories is allowed depending on the selected level of the guidance force (0–100%). Here, the guidance force was set to 100%, which guides legs with high impedance and results in the most constrained and consistent stepping pattern such that small deviations from the predetermined gait trajectories lead to larger corrective forces imposed by the actuators (Banz et al. 2008). The body-weight support, treadmill speed, and guidance force were kept constant throughout the recordings to minimize the impact of these variables on the outcomes of interest.

The participants were instructed and supervised by a research therapist to actively “walk with the robot” in a manner that would minimize robotic assistance (Riener et al. 2005; Koenig et al. 2011). The robot assists as needed, imposing corrective torques when necessary to maintain the predefined joint trajectories based on leg segment lengths and selected joint range of motion. These robotic torques were recorded during stepping with the built-in hip and knee sensors and later analyzed. The ankle joint was held with passive foot support, adjusted to keep the ankle in slight dorsiflexion to prevent toe drag during the swing phase of stepping.

Transcutaneous spinal stimulation setup

Two self-adhesive round hydrogel electrodes (5 cm diameter) were placed next to each other over the T11/12



interspinous space and connected to act as a single cathode. Two rectangular electrodes (7.5×10 cm) were placed over the lower anterior abdomen left and right of the umbilicus and connected as a single anode. Before the electrode placement, the skin was cleaned to reduce the electrode impedance.

A current-controlled stimulator (DS7A, Digi-timer North America LLC, Ft. Lauderdale, FL, US) was used to deliver 1-ms long monophasic rectangular pulses. The stimulator was triggered in real-time with a computer-controlled embedded data acquisition and control unit

Fig. 1 Recording setup and illustrative robotic torques and angles in participant S2 (left leg). Recording setup: The participant was placed in the robotic gait orthosis on a treadmill with body-weight support (Lokomat Pro, Hocoma, Inc.). Robotic torques and angles in hip and knee joints were outputted in real-time using the device's research software settings. EMG signals were simultaneously recorded in the rectus femoris (RF), medial hamstrings (MH), tibialis anterior (TA), and soleus (SO) muscles. During stepping at constant treadmill speed and body weight support, continuous transcutaneous spinal stimulation was applied at frequencies from 1 to 100 Hz and at constant intensity. **b** Superimposed angle (A) and torque (T) signals for five consecutive gait cycles (duration 2.4 s each) at different stimulation frequencies. Hip–knee cyclograms (top) show the gait trajectories of the robotic joints (beginning of stance, black circle; start of swing, gray circle). Hip (middle) and knee (bottom) robotic torques were recorded by joint sensors (stance phase, 62%, in black; swing phase, 38%, in gray). Note similar trajectories but changes in hip and knee torques at different stimulation frequencies. **c** Traces of stimulation frequencies (Freq) and relative changes in the hip ($r\Delta T_{Hip}$) and knee ($r\Delta T_{Knee}$) robotic torques over 310 gait cycles for stance (black) and swing (gray). Hip and knee robotic torques are normalized to the first ten gait cycles without stimulation. **d** The violin plots for the relative changes in hip and knee torques for each stimulation frequency bin during stance and swing. The mean and standard deviation are marked inside the violin plot. The standardized mean difference (SMD) greater than 1 (yellow) and less than -1 (blue) is indicated on the top of the violin plots

(CompactRIO Systems and LabVIEW 13.0, National Instruments Inc., Austin, TX, US). The proper placement of the cathode was confirmed by eliciting short-latency evoked responses in the supine position (Krenn et al. 2013, 2015; Sayenko et al. 2015).

Electrical stimulation during robot-assisted stepping

After placing the participant in the orthosis and checking the proper fit, the common motor threshold was determined by on-screen monitoring as the minimum intensity that evoked consistent low amplitude EMG responses in all recorded muscle groups (Minassian et al. 2007). The stimulation intensity was set individually to the highest level that was not evoking short-latency responses across the applied range of stimulation frequencies during weight-supported standing and could be tolerated throughout the experiment (Table 1, range 22–75% of the common motor threshold). The stimulation intensity was constant during the recordings, whereas the stimulation frequency was selected randomly from a quadratic space using Latin hypercube sampling (Loh 1996; Shields and Zhang 2016).

At the beginning of data collection, the robotic torques and EMG were first recorded without stimulation (10 gait cycles). Then, the stimulation frequencies (Table 1) from 1 up to 100 Hz were randomly selected by custom-made software and remained constant for either six (S2, S4, S7, S9) or ten (S1, S3, S5, S6, S8) consecutive gait cycles. Across individuals, the total number of unique stimulation frequencies examined ranged from 28 to 46 (Table 1). The

frequency change was accomplished by smoothly increasing or decreasing the frequency over one gait cycle, starting with the right heel strike defined by the Lokomat output signal. Stepping without stimulation was repeated randomly throughout the recording (range 20 to 84 gait cycles, median 30). In total, data from 310 consecutive gait cycles were analyzed, of which the first ten gait cycles without stimulation were used for normalization.

EMG and Lokomat data acquisition

Surface EMG sensors (MA-411, Motion Lab Systems Inc., Baton Rouge, LA, USA) were placed bilaterally over the rectus femoris (RF), medial hamstrings (MH), tibialis anterior (TA), and soleus (SO) muscles, midline along the most prominent portion of the muscle belly. Before placement, the skin was prepared with an abrasive paste (Nuprep Skin Prep Gel, Weaver and Company, Aurora, CO, US) to reduce electrode interface impedance. The active sensors had medical-grade stainless-steel electrode interfaces of two 12 mm disks at an inter-electrode distance of 17 mm and a pre-amplifier gain of 20 (MA-411, Motion Lab Systems, Inc., Baton Rouge, LA, US). The EMG signals were amplified using the MA-300 system (Motion Lab Systems, Inc., Baton Rouge, LA, US) with a total gain of 350 and a bandwidth from 10 Hz to 1 kHz.

The Lokomat analog module outputs included the robotic joint torques produced by the hip and knee actuators, the hip and knee joint angles, and the body-weight support. These signals were low-pass filtered with a 20-Hz Butterworth filter. The Lokomat and EMG signals were simultaneously digitized at 2000 samples per second (CompactRIO Systems).

Data processing and statistical analysis

The data processing and statistical analysis of robotic torques and EMG signals were performed in Matlab R2017b (MathWorks Inc., Natick, MA). Additional statistical tests were performed as indicated. The data set submitted to this analysis is available upon reasonable request.

Robotic torque analysis

Torque processing. For each joint (hip, knee) and side (left, right), the area under the curve of the robotic torque signal (Fig. 1b) was calculated for the stance phase and swing phase (62 and 38% of the gait cycle, respectively). A gait cycle was identified by the subsequent heel-strike signals from the output of the robotic gait orthosis. Subsequently, the relative change in torque ($r\Delta T_{gc}$, in %) was calculated as the normalized difference between the torque during each gait cycle (T_{gc}), and the averaged torque across the first ten

gait cycles without stimulation (T_{ini}) for each joint, side, and gait phase (Eq. 1).

$$r\Delta T_{gc} = \frac{T_{gc} - T_{ini}}{T_{ini}} \cdot 100 \quad (1)$$

Frequency grouping. Since the software randomly selected the stimulation frequency, the torque data for all corresponding gait cycles were grouped into eight bins: no stimulation, 1–5, 5–10, 10–20, 20–30, 30–50, 50–70, and 70–100 Hz (the higher bin value refers to “less than” except for 100 Hz). This grouping provided the most consistent bin size within and across the participants, with an average of 40.0 gait cycles (range 17–76; standard deviation, $SD=11.8$). Outliers within a bin were removed if the torque values exceeded six times the lower or upper semi-interquartile range measured from the median (Schwertman et al. 2004; Dovoedo and Chakraborti 2015), which occurred in 1.1% (248 instances) across all conditions.

Main outcome measure. The primary focus was on the change in the normalized robotic torque during stimulation compared to no stimulation. Therefore, we calculated the standardized mean difference (SMD) (Hedges' g , Eq. 2) between the average change in relative torque for each frequency bin ($r\Delta T_{gclfrq}$) and the average change in relative torque for the no stimulation bin ($r\Delta T_{gcl0}$), while accounting for the respective torque variance (s^2_{frq}, s^2_0) and sample size (n_{frq}, n_0) (Hedges et al. 2013). The torque data of each participant, joint, gait phase, side, and frequency bin was inspected for normality using a Q–Q plot and statistically analyzed by a one-sample Kolmogorov–Smirnov test (standard normal distribution in 542 out of 552 cases, 98.2%). SMD values were calculated according to the formula:

$$SMD_{frq} = \frac{\text{mean}(r\Delta T_{gclfrq}) - \text{mean}(r\Delta T_{gcl0})}{\sqrt{\frac{(n_{frq}-1)}{n_{frq}} s^2_{frq} + \frac{(n_0-1)}{n_0} s^2_0}} \quad (2)$$

Grouping of participants based on individual SMD profiles

An agglomerative clustering was used to determine similarities in individual SMD patterns based on calculating the Euclidean distance and Ward's linkage criterion (Luque-Casado et al. 2020). For this, the SMD values were averaged between the left and right sides for each condition to best approximate individual profiles. Due to missing data in three participants (S4, S7, S8), the 70–100 Hz frequency bin was excluded from this analysis. As shown in Eq. 3, the Euclidean distance ($ED_{i,j}$) was calculated between each pair of participants ($i, j: S1, \dots, S9$) using corresponding SMD values for each joint (jt: hip, knee), gait phase (gp: stance, swing), and frequency bin (frq: 1–5 Hz, ..., 50–70 Hz).

$$ED_{i,j} = \sqrt{\sum_{jt} \sum_{gp} \sum_{frq} (SMD_i - SMD_j)^2} \quad (3)$$

In the resulting dendrogram, the groups were identified using a dissimilarity cut-off value of 5 (Fig. 2b).

Within-group characterization of SMD classes between gait phases, joints, and sides. SMD values were aggregated into three classes for each group identified by cluster analysis (Fig. 3a) to emphasize large differences (i.e., effect size). The classes were defined as greater than +1 SMD, less than –1 SMD, and between +1 and –1 SMD. Within each cluster group, a 3-by-2 Chi-square test with Yates' correction (Preacher 2001) for continuity was used to determine whether the proportions of classes differed between stance/swing, hip/knee, and left/right sides across all frequency bins combined ($p < 0.05$).

Within-group characterization of SMD magnitude across frequency bins. A second-order polynomial regression (SPSS 27.0, IBM Inc., Armonk, NY) was used to determine the relationship between frequency bins (frq) and absolute SMD values within each group ($|SMD| = \beta_0 + \beta_1 * frq + \beta_2 * frq^2 + \epsilon$). The seven frequency bins were equidistantly dummy coded from –3 (1–5 Hz) to +3 (70–100 Hz), respectively. All available data points within a group were included in the analysis (joint, side, gait phase). The reported standardized coefficients (β_1^*, β_2^*) indicate the relative effect of the linear and quadratic terms in the polynomial regression (Fig. 3b).

EMG analysis

Detection and removal of stimulation artifacts. The stimulation artifacts were detected in the averaged EMG signal of the proximal muscles by identifying the data points that exceeded a 10-mV threshold, a value substantially larger than the ongoing EMG. An appropriate time window was selected for each muscle and participant, starting with a leading edge of the artifact and ending after 5–30 ms ($M=12.3$ ms, $SD=5.4$ ms) in the proximal muscles and after 2–30 ms ($M=7.8$ ms, $SD=6.4$ ms) in the distal muscles. The data points within the window were removed and set to Not-a-Number for subsequent analysis.

Individual EMG analysis. The artifact-free EMG was rectified, and a moving average of 100 ms was applied to derive the EMG envelope for each muscle. The EMG envelope was averaged across the entire gait cycle provided that more than 50% of data points remained after artifact removal (no data for 61 frequency bins, 11.1% across all participants, due to artifacts at higher frequencies).

The EMG data were analyzed in the same way as the torque data. The average EMG envelope data were aggregated for each frequency bin (including no stimulation).

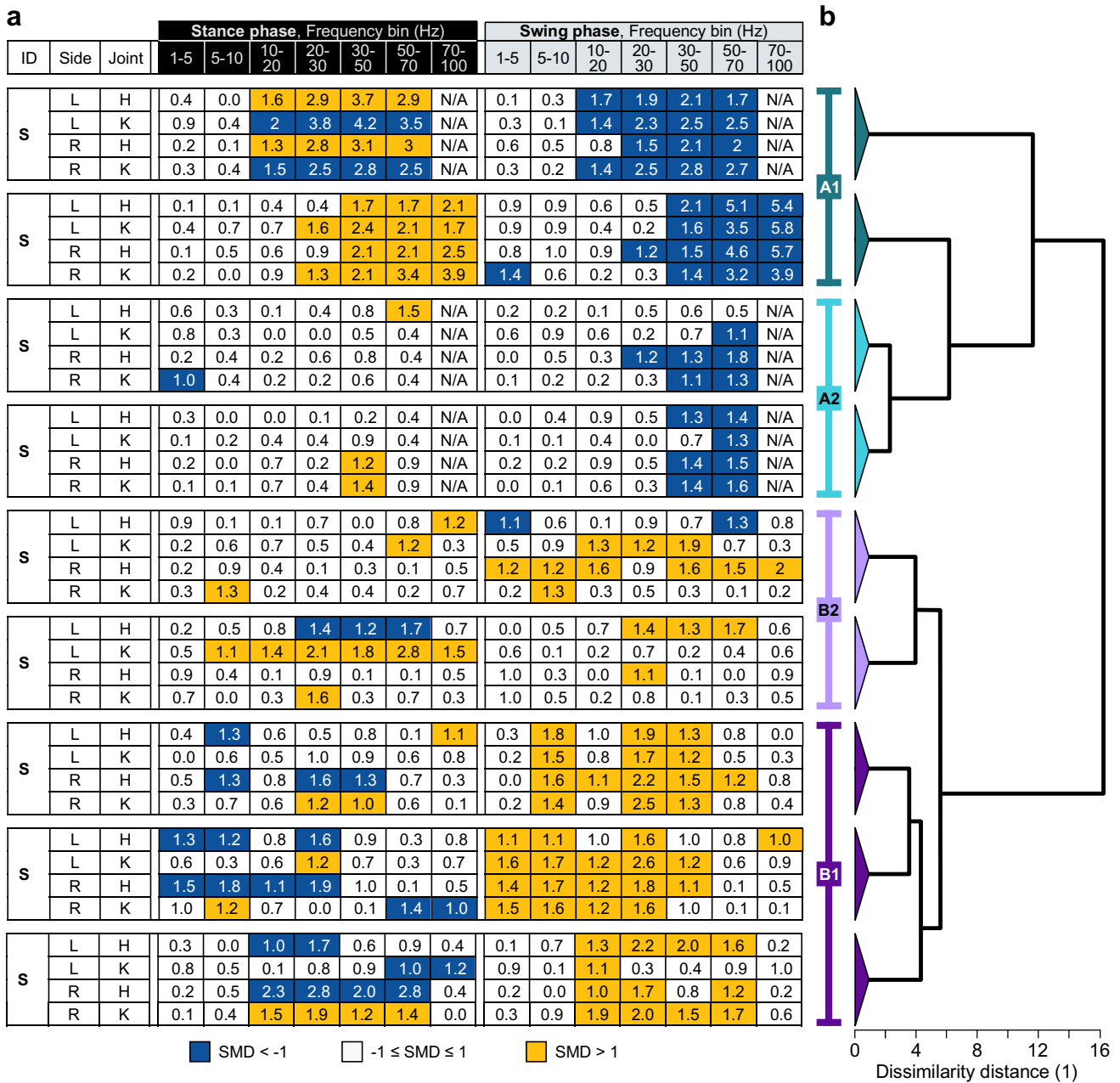


Fig. 2 Grouped standardized mean difference (SMD) of the robotic torques for all participants. The standardized mean difference (SMD) values across frequency bins are presented for each participant's gait phase, side, and joint. Positive SMD indicates a relative increase in robotic torque (values greater than +1 in yellow), and negative SMD indicates a relative decrease in robotic torque (values less than -1 in blue) compared to no stimulation condition. Abbreviations: L, left; R, right; N/A, not available. Note: The colored fields are mostly opposite for stance and swing within a given participant but not always in the same direction across participants (four participants blue in swing and five predominantly yellow in swing).

The outliers within each bin were excluded (1.1% of all data, 192 outliers). The SMD values were calculated based on the mean and standard deviation for each stimulation frequency bin in relation to the no stimulation bin (Eq. 2) to avoid over-interpretation of small variations in EMG. The change in muscle activity during TSS was considered

meanings: L, left; R, right; N/A, not available. Note: The colored fields are mostly opposite for stance and swing within a given participant but not always in the same direction across participants (four participants blue in swing and five predominantly yellow in swing). **b** The dendrogram shows the grouping of the participants based on the SMD patterns with four groups identified: A1 (S7, S2), A2 (S8, S4), B2 (S1, S3), and B1 (S5, S9, S6)

meaningful if the SMD values were greater than +1 or less than -1.

Contribution of short-latency responses to gait-related EMG. Short-latency responses were identified to account for their contribution to the EMG envelope. Therefore, we averaged the EMG signal within a window of 21.1 and 20.3 ms

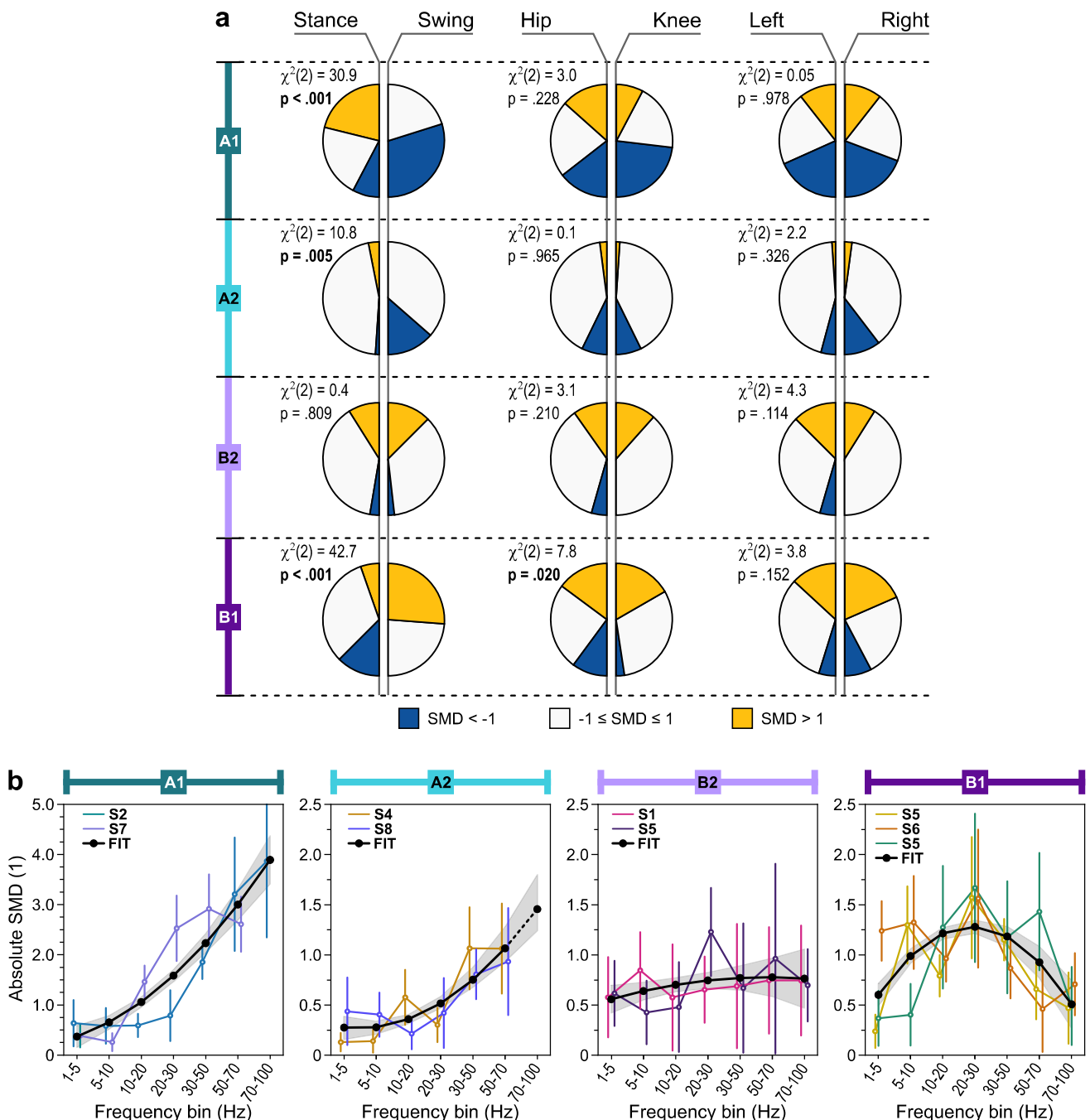


Fig. 3 Analysis of grouped standardized mean difference (SMD) torque profiles. For each group, the half-circles show the proportions of SMD values greater than +1 (yellow), less than -1 (blue), and between -1 and 1 (white) for stance vs. swing (left column), hip vs. knee joints (middle column), and left vs. right sides (right column). The Chi-square results test the distribution of three SMD classes over two gait phases, joints, and sides (significant difference in bold). Note that the proportion of the SMD values is significantly different between the stance and swing across the groups (first column). **b** The absolute SMD values averaged across stance/swing, hip/

knee, and left/right sides are presented for each frequency bin and participant (lines in color, error bar shows SD, first panel with a different y-axis scale). The black line presents the best fit of a quadratic polynomial function across all data points in each group (gray area indicates a 95% confidence interval). For group A2, a dotted line represents the extrapolation of the polynomial function to the 70–100 Hz bin for which data were missing. Note a larger increase in the absolute SMD value with the stimulation frequency in groups A1 than A2, no change in group B2, and the inverted U-shape profile in group B1 peaking at 20–30 Hz

in the proximal and distal muscles, respectively, starting at 14.3 ($SD=4.3$) ms and 20 ($SD=0$) ms from the stimulation onset across all frequencies up to 50 Hz (higher frequencies not included here due to overlapping responses). Short-latency responses were considered prominent if two criteria were met: the peak-to-peak amplitude of the averaged EMG signal was larger than 50 μ V and the ratio between the root mean square value of the averaged and the ongoing EMG signal was larger than 0.50. When both criteria were met, the presence of short-latency responses within the EMG envelopes was designated as such for all studied frequency bins to facilitate the interpretation of the results.

Results

Changes in robotic torques during stepping with TSS

Examples of relative changes in the robotic torques ($r\Delta T$) are shown in Fig. 1b–d for the entire recording session (310 gait cycles) without and with TSS applied at randomly selected stimulation frequencies in participant S2 (left leg). Administering the stimulation at different frequencies produced rapid changes in torque that were sustained mainly in magnitude over multiple gait cycles (Fig. 1c). The changes in robotic torques during stimulation were predominantly in opposite directions between stance (positive SMD values) and swing (negative SMD values) in both hip and knee joints (Fig. 1c). With frequency data aggregated in bins, it became apparent that the hip and knee robotic torques increased during stance and decreased during swing at higher frequencies in this participant (Fig. 1d). The SMD values indicated approximately 2–3 times larger changes in robotic torques during swing than stance at high frequencies.

The robotic torques for no stimulation (control condition), interspersed throughout the recording session, were consistent (see example in Fig. 1b, first and last column). Across all participants, the absolute difference between the first ten gait cycles and the last gait cycles without stimulation was on average 8.7%, ranging from 1.6 to 15.0%.

Figure 2a presents the SMD values for each participant across stimulation frequency bins for stance/swing, hip/knee, and left/right side. The SMD values exceeding ± 1 SMD were presented in color. The magnitude and direction of SMD values indicate heterogeneous changes in torque during stimulation among the participants.

Clustering of individual SMD-torque profiles

Agglomerative clustering determined the grouping of participants based on similarities of individual SMD-torque profiles during stimulation. Based on the Euclidian distance, two main groups (A, B) were identified with two sub-groups each (1, 2). The dendrogram shown in Fig. 2b had a cophenetic correlation coefficient of 0.65, indicating a moderately faithful representation of dissimilarities among observations (Mukaka 2012; Saraçli et al. 2013). Group A included participants S2, S4, S7, and S8, and group B participants were S1, S3, S5, S6, and S9. Further subgrouping was based on a cut-off dissimilarity value of 5, resulting in two singletons combined into group A1 and three other groups, A2, B1, and B2. The grouping order in the dendrogram, A1 (S2, S7), A2 (S4, S8), B2 (S1, S3), and B1 (S5, S6, S9), was selected to emphasize extremes, i.e., larger average absolute SMD values for the sub-groups A1 and B1 than A2 and B2.

Group features based on SMD classes

Figure 3A presents the distribution of the three categories of SMD values (less than –1, between –1 and +1, greater than +1) across two gait phases, joints, and sides in each group identified by the cluster analysis. The results of the chi-square test of independence with Yates' correction were used to determine whether the pattern (proportions) of SMD classes differed between stance/swing, hip/knee, and left/right sides, as described below.

Stance vs. swing phase (Fig. 3a, left). The proportions of SMD classes differed significantly between stance and swing in groups A1, A2, and B1 (Cramer's $V=0.54$, 0.34, 0.50, respectively) but not in group B2 (Cramer's $V=0.09$). In group A1, SMD values greater than +1 (yellow) occurred more often in stance (42%) than swing (0%), whereas SMD values less than –1 (blue) were more prevalent in swing (56%) than stance (29%). This suggested that in group A1 the robotic torque during stimulation predominantly increased in stance and decreased in swing. The opposite trend was observed for group B1, with 52% of SMD values greater than +1 occurring in swing and only 11% in stance, whereas 25% of SMD values less than –1 were found in stance but 0% in swing.

Hip vs. knee joint (Fig. 3a, middle). A significant difference between the joints was only observed in group B1 ($p=0.010$) due to a greater proportion of SMD values less than –1 occurring in the hip (20%) than in the knee (5%). However, the effect was small (Cramer's $V=0.22$). No significant differences in the remaining groups were found.

Left vs. right side (Fig. 3a, right). The proportions of SMD classes were not significantly different between the right and left sides for any group, suggesting no differences in the left/right pattern of robotic torque changes. This supported the decision to average SMD values between the two sides for the cluster analysis.

Group features of SMD magnitude across frequency bins

Figure 3B presents a frequency-dependent profile of SMD magnitude (absolute values) for each participant within the four groups. The quadratic regression model was statistically significant for group A1 ($F(2, 101)=88.9, p<0.001; R^2=0.64$), group A2 ($F(2, 93)=31.0, p<0.001; R^2=0.40$), and group B1 ($F(2, 165)=21.6, p<0.001; R^2=0.21$) but not for group B2 ($F(2, 109)=1.1, p=0.349; R^2=0.02$).

Groups A1 and A2 showed a monotonic increase in SMD magnitude from low to high stimulation frequencies at a rate that was about three times greater in A1 than in A2 (non-standardized β_1 0.59 and 0.20, respectively). The standardized coefficients for the linear and quadratic terms for groups A1 and A2 were similar, however; $\beta_1^*=0.82$ ($p<0.001$) and $\beta_2^*=0.15$ ($p=0.018$) for group A1, and $\beta_1^*=0.74$ ($p<0.001$) and $\beta_2^*=0.26$ ($p=0.009$) for group A2. Larger β_1^* than β_2^* coefficients indicated a predominant linear change in robotic torque across the frequency bins in both groups A1 and A2.

In contrast, group B1 showed an inverted U-shaped frequency profile with the maximum SMD magnitude in the mid-frequency range (20–30 Hz). This was consistent with a larger quadratic ($\beta_2^*=-0.45, p<0.001$) than linear standardized coefficient ($\beta_1^*=-0.05, p=0.464$). The quadratic regression for group B2 was not significant ($\beta_1^*=0.13, p=0.191; \beta_2^*=-0.06, p=0.530$), suggesting no distinct change in robotic torques across stimulation frequency bins.

Muscle activation during robotic stepping

EMG from proximal and distal flexors and extensors was collected simultaneously with the torques. Figure 4 shows the means and SDs for the average EMG envelope during the gait cycle across stimulation frequency bins for participants in each group for the left and right side, separately. Changes in EMG exceeding ± 1 SMD occurred in multiple muscles (Fig. 4, circles) in group A (41.3% total) and group B (49.8% total). Consistent short-latency responses evoked by TSS were detected in 5 (7.1%) proximal muscles and 2 (2.9%) distal muscles out of 70 available muscle recordings (Fig. 4, dash line). At higher stimulation frequencies, these evoked responses contributed to the increase in EMG envelope (SMD larger than +1). Moreover, groups A1, A2, B2,

and B1 exhibited different patterns of EMG changes across the stimulation frequencies.

In group A1 (Fig. 4, first column), the most pronounced changes in EMG were at higher frequencies. In participant S7, there was about a 50% decrease in EMG in both SO muscles starting at 10–20 Hz. Figure 5 presents the EMG traces of five consecutive gait cycles in the right leg muscles in participant S7 for no stimulation and three stimulation frequencies (9, 24 and 50 Hz). Both SO and TA muscles showed consistent clonogenic motor output (hereafter “clean” for brevity) without stimulation at the beginning and later in the recording session that was reduced at 24 and 50 Hz stimulation. The gait-related EMG envelopes decreased in both proximal and distal muscles at these same frequencies. Also, in participant S2, both clonus in the right SO and gait-related EMG in the right MH were decreased at 30 Hz and above (Fig. 4, first column). The observed increase in EMG in select muscles (RF-R, TA-L muscles in S7, RF-R in S2) was predominantly associated with the appearance of the short-latency evoked responses across the broad range of frequencies.

In group A2 (Fig. 4, second column), the pattern of changes in EMG was similar to that in group A1; the decrease in EMG envelope occurred in the same frequency range (30–50 Hz), but the change was of lesser magnitude. The increase in the EMG envelope was mainly associated with the presence of short-latency responses. In group B2, inconsistent or negligible changes in EMG were found (Fig. 4, third column).

In group B1 (Fig. 4, last column), when the EMG was present without stimulation, it increased with TSS in the mid-frequency range. This EMG increase was not associated with the presence of short-latency evoked responses except in one muscle (S9-R, RF). The EMG traces for participant S6 (Fig. 6) reveals an increase in gait-related muscle activity in all muscles at 33 Hz (Fig. 6). A similar EMG increase in the mid-frequency range was observed in both MH muscles in participant S5 (Fig. 4), mainly during the swing phase. In participant S9, however, the EMG increase in the right TA and SO was related to the increase in clonus (examples at 22 and 49 Hz presented in Fig. 7), which disappeared at higher frequencies. Also, short-latency responses contributed to the increased EMG in the right RF.

Discussion

We examined the immediate effect of continuous TSS across different stimulation frequencies on robotic torques in the hip and knee joints and muscle activation patterns in the lower limbs during treadmill stepping. Agglomerative clustering returned four groups that differed in the sign and magnitude of changes in robotic torques during stance and

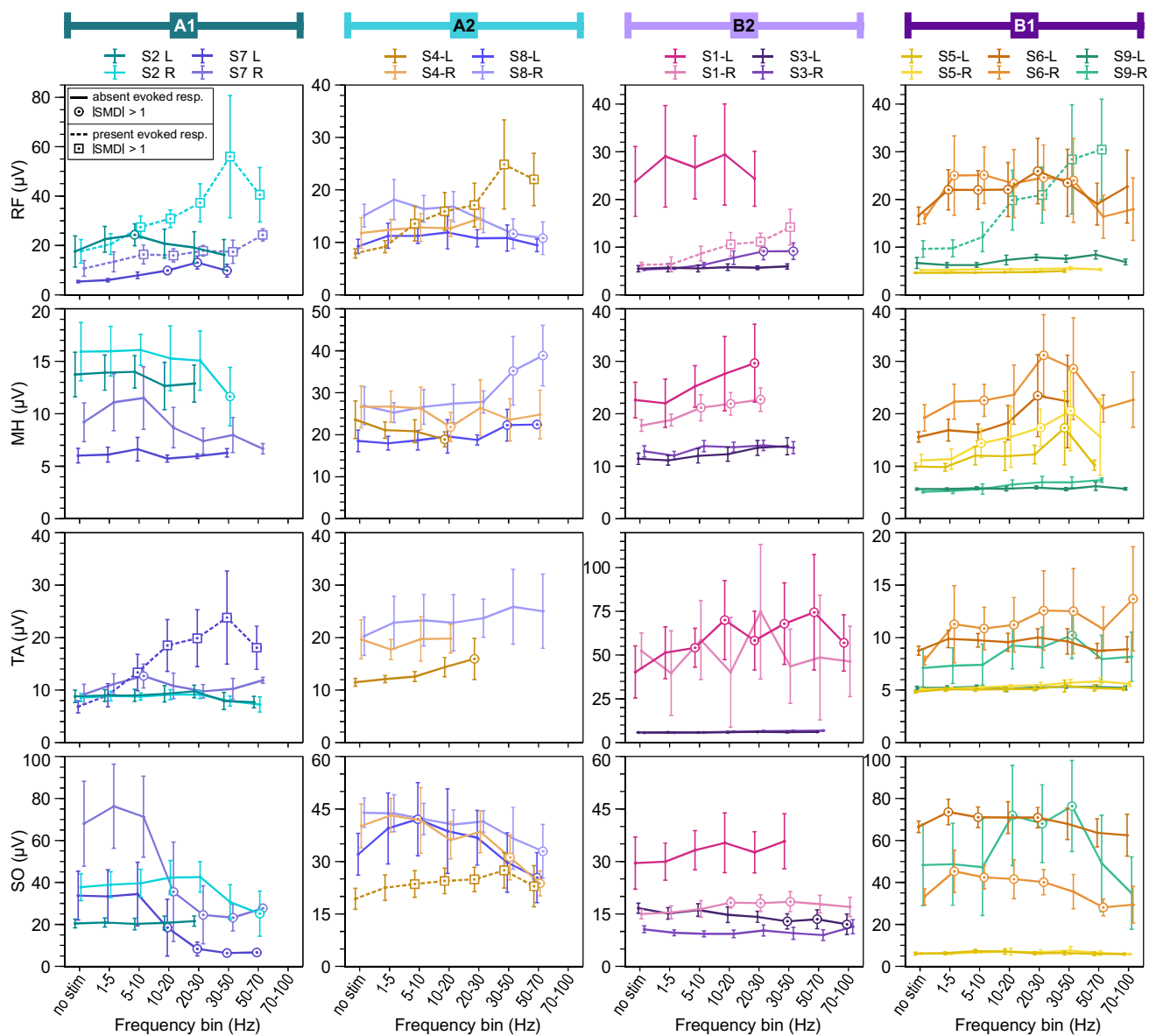


Fig. 4 Mean (SD) values of the EMG envelopes over the entire gait cycle for each frequency bin in the rectus femoris (RF), medial hamstrings (MH), tibialis anterior (TA), and soleus (SO) for each group (columns) and individual participants for the left (L) and right (R) leg. A circle represents SMD values greater than +1 or less than -1.

The dashed lines indicate TSS short-latency evoked responses superimposed on the gait-related EMG. The data points missing at higher frequencies are due to excessive data loss after removing stimulation artifacts. Data in S9-L (SO) and S8-L (TA) are missing due to EMG sensor error

swing depending on the stimulation frequency. In groups A1 and A2, with increased stimulation frequency, the robotic torques changed progressively more, indicating greater deviations from the pre-specified joint angles during stimulation, which coincided with a decrease in muscle activation, mainly attributed to reduced clonus in the lower leg muscles. In group B1, the change in robotic torque at increasing frequencies followed an inverted u-shape, which coincided with an increase in muscle activation over the mid-frequency range, reflecting the augmentation of either gait-related physiological output or pathophysiological output. The

selected torque and EMG outcomes did not reveal a clear pattern of changes in group B2. The association between the stimulation frequency and changes in robotic torques during stance and swing were largely opposite between the groups A1/A2 and B1/B2. In summary, this study demonstrates different frequency and gait phase-dependent motor profiles during robot-guided stepping in humans with incomplete spinal cord injury.

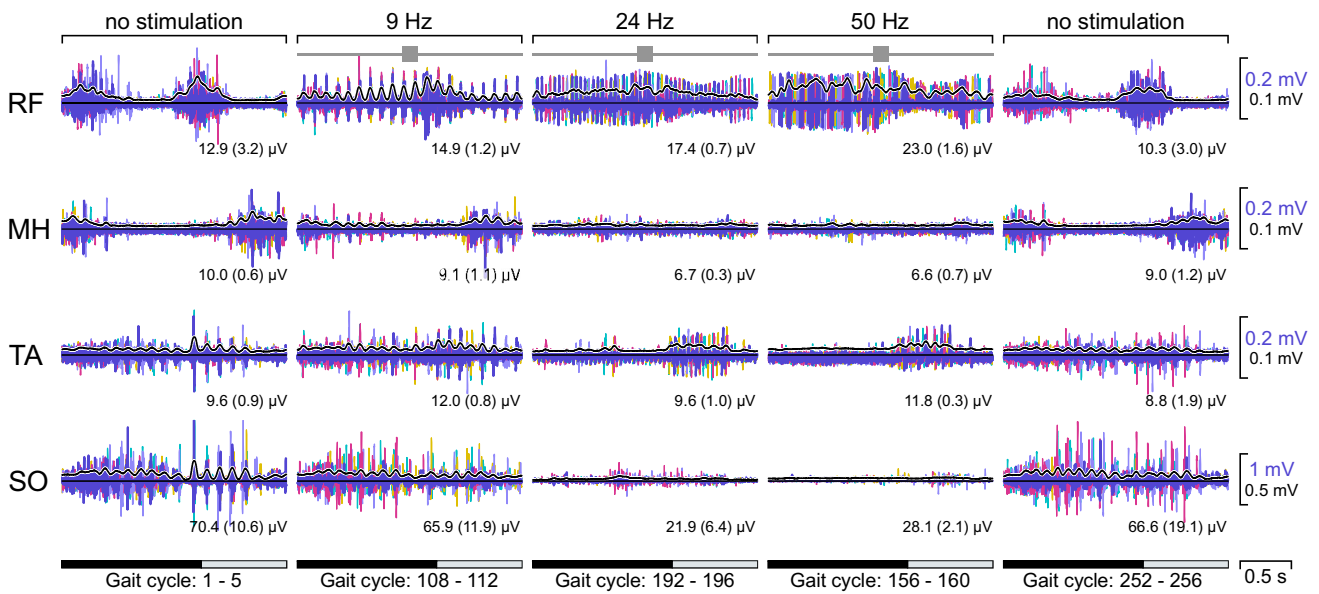


Fig. 5 EMG signals of five consecutive gait cycles for select stimulation frequencies in participant S7 (group A1). Superimposed EMG traces are shown in different colors (stimulation artifacts removed), and the average EMG envelope is black (the respective scales are shown in color and black). The mean values (SD) of the EMG envelope for the gait cycle are presented under each trace. The gait phase

(stance, black; swing, gray) and gait cycle numbers are indicated at the bottom of each panel. Muscles: *RF* rectus femoris, *MH* medial hamstrings, *TA* tibial anterior, *SO* soleus (right leg, in all cases). Note EMG suppression in *MH* and *TS* at higher stimulation frequencies. The increase in EMG in *RF* is due to more frequent evoked responses (*).

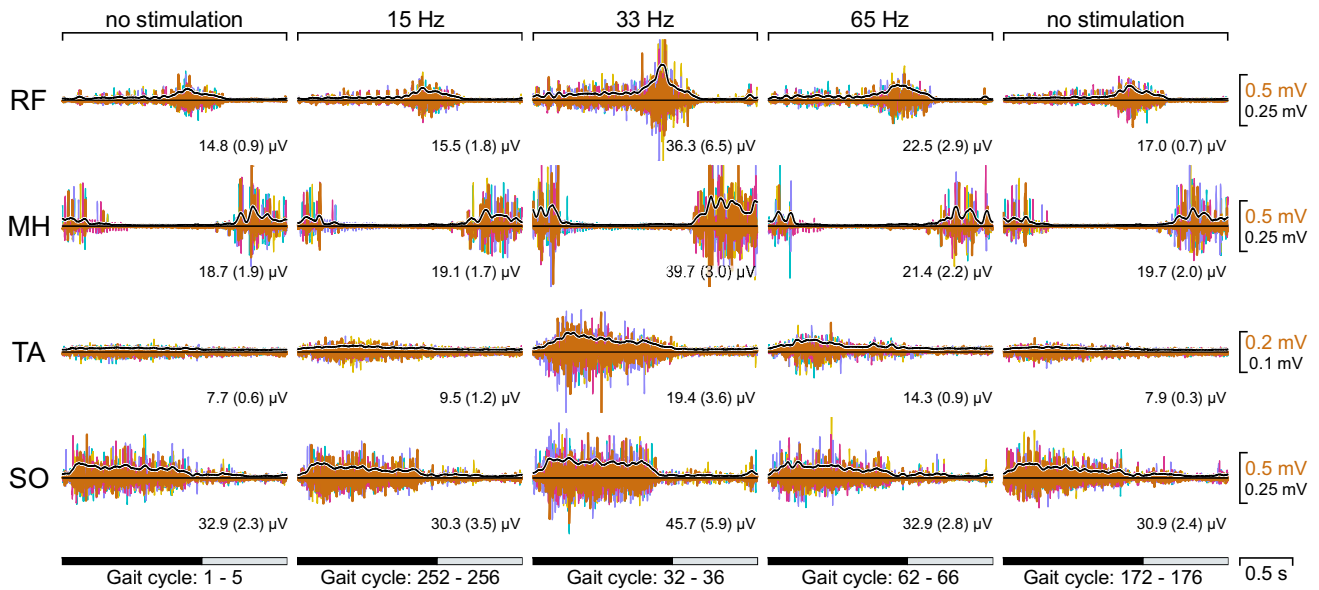


Fig. 6 EMG signals of five consecutive gait cycles for select stimulation frequencies in the right leg of participant S6 (group B1). See Fig. 5 legend for details. Note that EMG in all the muscles waxes and then wanes as frequencies increase, with a peak at 33 Hz

Effect of TSS on robotic torques varies across participants

The direction and magnitude of change in robotic torques during TSS varied visibly across the nine participants and

more so between frequencies and gait phases than joints and sides (Fig. 3a). This suggests that a “one size fits all” approach to the therapeutic application of continuous TSS is not likely to serve all SCI patients equally well, at least not for achieving consistent stepping. This is not

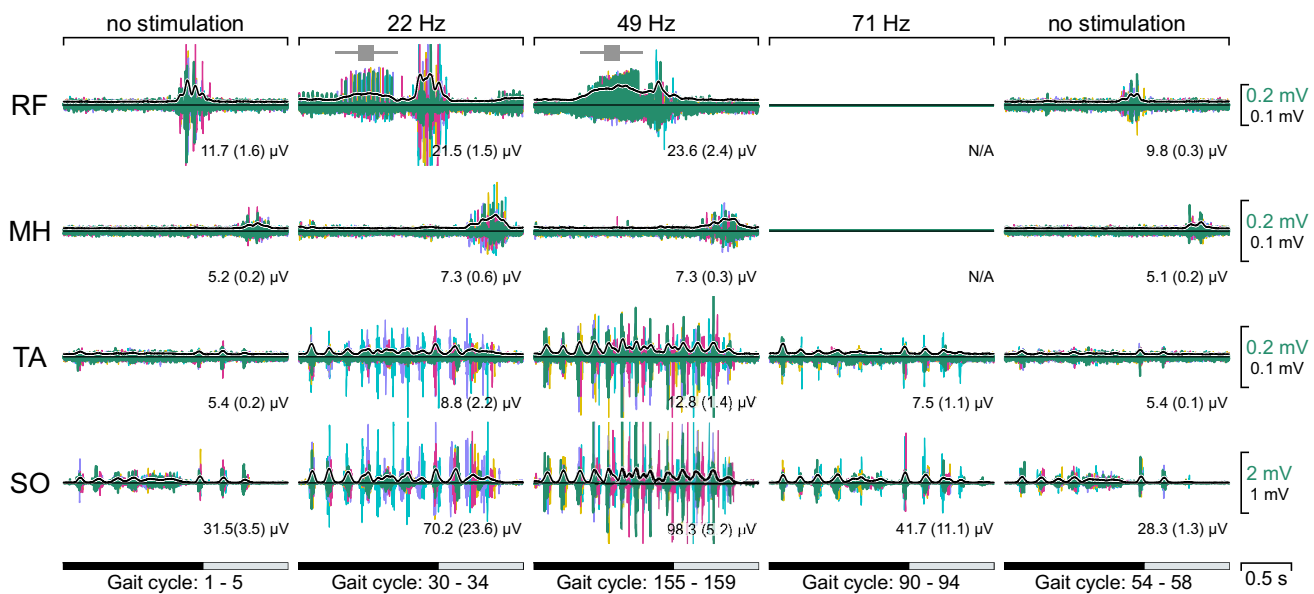


Fig. 7 EMG signals of five consecutive gait cycles for select stimulation frequencies in the right leg of participant S9 (group B1). See Fig. 5 legend for details. Note the increase in clonus up to 49 Hz followed by the decrease at higher frequencies. The increased EMG in

RF is due to more frequent evoked responses (*) during the stance phase. N/A, trace not shown due to excessive stimulation artifacts at higher stimulation rates

surprising given that the capacity for stepping is expected to be heterogeneous in individuals with diverse levels and severities of SCI, as recruited here. The common clinical descriptors of SCI (Table 1) could not discriminate different capacities for stepping in the robotic orthosis or responses to TSS. This further speaks to the need for additional or other means (clinical, behavioral, neurophysiological, etc.) of profiling patients to predict responses to stimulation intervention. Also, the observed spectrum of responses suggests the value of obtaining complementary measurements during a target behavior, such as robotic torques and EMG during stepping as in this study, and the potential role for powered robotic orthoses in studying the effects of spinal stimulation on various motor functions, like standing, maintenance of balance, or spasticity control.

Effect of TSS on robotic torques is related to the gait phase

Agglomerative clustering identified different profiles across the participants in this study with the most distanced groups, A1 and B1, characterized by the large and opposite changes in torque ($|SMD\text{-value}| > 1$) during TSS in the stance and swing phase (A1: torques decrease in stance and increase in swing, B1: torques increase in stance and decrease in swing). While group A2 followed the same pattern as seen in A1, B2 did not show a difference between the two gait phases (Fig. 3a). Therefore, for groups A1 and A2, the hip and knee

joint angles during TSS were closer to the predetermined trajectories in stance and further away during swing, whereas the opposite was the case for group B1.

In none of the participants, neuromodulation consistently reduced or increased robotic torques across the entire gait cycle at all joints and stimulation frequencies. This suggests that the effects of continuous stimulation may be more complex than simply increasing or decreasing the excitability of spinal circuitry below the level of injury. While the spinal cord can show the capacity for transforming continuous peripheral input into phasic output (Dimitrijevic et al. 1998; Danner et al. 2015), this may not be expressed easily or in the adequate muscle activation pattern in motor incomplete SCI. This means we should not always count on intraspinal circuitry to integrate continuous multi-segmental afferent input with the supraspinal input to improve stepping in incomplete injury. Thus, alternative stimulation strategies may be needed to distribute input across different spinal levels and phases of the gait cycle (Wagner et al. 2018; Rowald et al. 2022).

Frequency-dependent profiles of changes in torque

The premise of the presented work is that TSS can modulate locomotor output during stepping over a wide range of stimulation frequencies, prompting us to examine random frequencies from 1 Hz up to 100 Hz. The studied frequency range covers the described effects of ESS and TSS for various applications (enabling standing, augmenting stepping,

suppressing spasticity), which may affect motor activity associated with gait. Several previous ESS (Angeli et al. 2014, 2018; Gill et al. 2018; Darrow et al. 2019) and TSS (Gerasimenko et al. 2015a; Hofstoetter et al. 2015; Meyer et al. 2020; McHugh et al. 2020) studies used frequencies in the range of 25 to 50 Hz over multiple sessions, with or without gait training, to improve locomotor output or gait performance. The implicit assumption and subsequent implications of these prior studies are that the stimulation frequencies with the greatest effect on stepping are within this narrow range. Our study, however, reveals effects on robotic torques that are more graded across stimulation frequencies. Specifically, in groups A1 and A2, the greatest absolute torque changes occurred at frequencies higher than 50 Hz, whereas in group B1, the initial rise in torque peaked at 20–30 Hz, followed by a decline above 30 Hz. As for group B2, the overall effect was modest, making this group poorly responsive to changes across the wide range of TSS frequencies under our experimental conditions.

Similar to our objective, a recent study (Meyer et al. 2020) contrasted the immediate effects of TSS at frequencies of 15, 30, and 50 Hz. Although no single frequency was superior to others for improving gait kinematics and EMG during overground walking across the group of six participants, some individual changes in the swing/stance and muscle activation profiles were reported. Our previous investigation at the same institution also demonstrated individually variable EMG patterns during 30-Hz robot-assisted stepping among four clinically complete SCI participants (Minassian et al. 2016). The collective evidence implies the intuitive prediction of divergent responses to neuromodulation regardless of the motor behavior studied. Thus, future work should focus on better profiling individuals to stratify their responses rather than expecting consistent responses across the individuals.

Interpretation of robotic torque

This study used torques recorded by the sensors in the robotic hip and knee joints to derive an outcome measure that reflects changes in human/robot interactions during guided stepping with TSS relative to no stimulation. These torques indicate corrective actions of the actuators such that the actual hip and knee joint angles are brought to alignment with the pre-specified joint angles at the rate dependent on the selected guidance force (here 100%, prompt correction upon detected deviation). We extracted the profiles of individual changes during the experiment by first normalizing the recorded robotic torques relative to the first ten steps without stimulation. Then we calculated a standardized mean difference of the area under the torque curve for each frequency bin between the bins of selected stimulation frequencies and no stimulation condition interspersed

throughout (control). Our outcome measure is equivalent to the effect size in statistics and indicates the magnitude of the experimental effect during the exposure to TSS at different frequencies.

The negative change in our outcome measure indicates that the actual joint angle in the stance and swing was overall closer to the pre-specified joint angle with TSS than without TSS and vice versa for the positive change (actual joint angle deviated more from the pre-specified joint) (Banz et al. 2009). Although the direction of change does not inform whether the actual angle was ahead or behind the pre-specified angle because both require equal corrective action, some inferences can be drawn based on different scenarios. For example, higher robotic torques may be needed to augment weakened movements or overcome increased stiffness during TSS; both can increase the deviation of the joint angle to the predefined trajectory. Conversely, lower robotic torques during TSS may be associated with stronger and better-timed voluntary movements or reduced limb stiffness and spasms that no longer impede or slow down the joint motion along the predefined trajectory. Since many people with motor incomplete SCI develop highly individual locomotor strategies, which can differ substantially from those observed in uninjured individuals, a potential TSS-related improvement in voluntary motor control may still lead to increased robotic torques to strictly follow the predefined movement trajectories.

Frequency-dependent profiles of changes in EMG

The two most distinct patterns of changes in motor output with TSS were the decrease in gait-related EMG and clonus at high frequencies (group A1) and the increase in EMG and the appearance of clonus in the mid-frequency range (group B1). Indeed, no participant showed an increase in EMG (physiological or pathophysiological) in mid-frequencies and a decrease in EMG at high frequencies. Moreover, we could not identify a specific frequency range that simultaneously augmented physiological output and reduced pathophysiological output, a highly desired outcome. These observations have several implications. First, the effect of low-intensity continuous TSS on gait-related EMG seems to be rather global and probably mediated through widespread changes in spinal excitability, as proposed before (Mayr et al. 2016). Second, the desired motor output may not be achieved just by modulating the frequency of TSS during gait. Most importantly, the individual effects across a wide range of frequencies seem to be mainly dependent on the motor profile such that excessive motor output can be tamed or weak motor output augmented. Thus, due to the heterogeneity of motor profiles in individuals with SCI, it is unlikely that the low-intensity continuous TSS can be

prescribed in the same way to all with the expectation of achieving uniformly favorable gait motor output.

Our observation of TSS augmenting physiological output is in accord with earlier observations (Hofstoetter et al. 2015; Gerasimenko et al. 2015b; Gad et al. 2017). However, we also provided evidence that stimulation in the range of 10–50 Hz can also augment pathophysiological output (clonus). This suggests that even low-intensity continuous TSS may have undesired effects in some individuals. The appearance of clonus seems inconsistent with the report that continuous electrical stimulation above 30 Hz blocks a significant amount of proprioceptive input in humans (Formento et al. 2018), but this may be due to the low-intensity stimulation used here.

In general, the pattern of changes in EMG agrees with the changes in robotic torque (Fig. 3b) across the range of studied frequencies. Specifically, the largest changes in torque and EMG were observed at high frequencies in groups A1 and A2, whereas the same was found at mid-frequencies in group B1. Neither torque nor EMG prominently changed in group B2. Furthermore, the disappearance of clonus with TSS was associated with the decrease in hip and knee torques during swing, whereas the increase in clonus was associated with the increase in hip and knee torques during the swing (Figs. 2, S2/S7 and S9, respectively). Assuming that the disappearance of clonus with TSS implies less prominent spastic motor behaviors, smaller robotic torques would be necessary to advance the leg throughout swing (S2, S7) and vice versa (S9). At the same time, more robotic torque would be needed to support body weight in stance.

Limitations

The analysis was done on over 310 gait cycles; the number settled on was large enough to probe the effect of many different stimulation frequencies selected randomly and changed every 6–10 steps. Walking continuously could produce fatigue, discomfort, and inconsistent engagement possible because of the constant support provided by the robotic orthosis. However, we compared robotic torques and EMG without stimulation both at the beginning and throughout the data collection and found negligible differences between the epochs of no stimulation. This suggests sufficiently stable conditions throughout the experimental session. Also, all epochs of no stimulation were used as a control condition against which the exposure to TSS was examined, which would account for possible variability over time. Finally, the analyzed number of steps per frequency bin is sufficiently large and consistent with the number typically recorded in treadmill and overground gait studies. It remains unknown, however, how our results relate to stimulation effects at specific frequencies over many more gait cycles.

The stimulation intensity was not consistent across the participants. While we initially aimed at 80% of the common motor threshold established in standing, we did not reach this level in most participants due to discomfort. This is a known limitation of TSS and possibly a reason to favor epidural stimulation in the long run. Even with the stimulation intensities used, occasional short-latency responses were detected in proximal muscles, which were accounted for to avoid overestimating the EMG envelope results. We believe this was a prudent and conservative approach that has not been used in previous similar studies.

Conclusion

Our study demonstrated different patterns of changes in robotic torque and muscle activation when low-intensity continuous TSS was applied to motor incomplete SCI individuals at frequencies from 1 to 100 Hz while stepping in a robotic gait orthosis. This suggests that individuals with SCI may respond differently to a single TSS frequency and, therefore, single-frequency treatment protocols are unlikely to be consistently successful across the injured population. To move in the right direction, better profiling of SCI individuals is needed to determine both the magnitude and pattern of TSS effects before applying this type of neuromodulation for improving gait in motor incomplete SCI.

Acknowledgements We thank Joy Bruce, Barry McKay, and Brad Farrell for their assistance with data collection.

Author contributions MJK: data curation, formal analysis, funding acquisition, methodology, software, validation, visualization, writing—original draft, writing—review and editing. JMW: data curation, investigation, methodology, software, validation, writing—review and editing. DSS: formal analysis, methodology, validation, visualization, writing—original draft, writing—review and editing. KET: conceptualization, funding acquisition, investigation, methodology, project administration, resources, supervision, visualization, writing—original draft, writing—review and editing.

Funding This study was supported by NIH NINDS (EB006179), the Shepherd Center Hulse Spinal Cord Injury Lab (SCIL) founding grant, Georgia Institute of Technology Graduate Programs, the Wings for Life—Spinal Cord Research Foundation (WFL-US-07/19:199), and The Yerger NeuroRobotics Research Fund and Wilson Research Foundation affiliated with Methodist Rehabilitation Center, Jackson, MS, USA.

Data availability The data set submitted to this analysis is available upon reasonable request.

Declarations

Conflict of interest MJK, JMW, and DSS declare no conflicts of interest. KET serves as a consultant for ONWARD Medical BV (Eindhoven, Netherlands).

References

- Adams MM, Hicks AL (2005) Spasticity after spinal cord injury. *Spinal Cord* 43:577–586. <https://doi.org/10.1038/sj.sc.3101757>
- Al'joboori Y, Massey SJ, Knight SL et al (2020) The Effects of adding transcutaneous spinal cord stimulation (tSCS) to Sit-To-stand training in people with spinal cord injury: a pilot study. *J Clin Med*. <https://doi.org/10.3390/jcm9092765>
- Angeli CA, Edgerton VR, Gerasimenko YP, Harkema SJ (2014) Altering spinal cord excitability enables voluntary movements after chronic complete paralysis in humans. *Brain* 137:1394–1409. <https://doi.org/10.1093/brain/awu038>
- Angeli CA, Boakye M, Morton RA et al (2018) Recovery of over-ground walking after chronic motor complete spinal cord injury. *N Engl J Med* 379:1244–1250. <https://doi.org/10.1056/NEJMoa1803588>
- Banz R, Bolliger M, Colombo G et al (2008) Computerized visual feedback: an adjunct to robotic-assisted gait training. *Phys Ther* 88:1135–1145. <https://doi.org/10.2522/ptj.20070203>
- Banz R, Bolliger M, Muller S et al (2009) A method of estimating the degree of active participation during stepping in a driven gait orthosis based on actuator force profile matching. *IEEE Trans Neural Syst Rehabil Eng* 17:15–22. <https://doi.org/10.1109/TNSRE.2008.2008281>
- Beres-Jones JA, Harkema SJ (2004) The human spinal cord interprets velocity-dependent afferent input during stepping. *Brain* 127:2232–2246. <https://doi.org/10.1093/brain/awh252>
- Calvert JS, Grahn PJ, Strommen JA et al (2019) Electrophysiological guidance of epidural electrode array implantation over the human lumbosacral spinal cord to enable motor function after chronic paraparesis. *J Neurotrauma* 36:1451–1460. <https://doi.org/10.1089/neu.2018.5921>
- Cuellar CA, Mendez AA, Islam R et al (2017) The role of functional neuroanatomy of the lumbar spinal cord in effect of epidural stimulation. *Front Neuroanat* 11:1–17. <https://doi.org/10.3389/fnana.2017.00082>
- Danner SM, Hofstoetter US, Freundl B et al (2015) Human spinal locomotor control is based on flexibly organized burst generators. *Brain* 138:577–588. <https://doi.org/10.1093/brain/awu372>
- Darrow D, Balser D, Netoff TI et al (2019) Epidural spinal cord stimulation facilitates immediate restoration of dormant motor and autonomic supraspinal pathways after chronic neurologically complete spinal cord injury. *J Neurotrauma* 36:2325–2336. <https://doi.org/10.1089/neu.2018.6006>
- Dietz V, Fouad K (2014) Restoration of sensorimotor functions after spinal cord injury. *Brain* 137:654–667. <https://doi.org/10.1093/brain/awt262>
- Dietz V, Sinkjaer T (2007) Spastic movement disorder: impaired reflex function and altered muscle mechanics. *Lancet Neurol* 6:725–733. [https://doi.org/10.1016/S1474-4422\(07\)70193-X](https://doi.org/10.1016/S1474-4422(07)70193-X)
- Dimitrijevic MR, Gerasimenko Y, Pinter MM (1998) Evidence for a spinal central pattern generator in humans. *Ann N Y Acad Sci* 860:360–376. <https://doi.org/10.1111/j.1749-6632.1998.tb09062.x>
- Domingo A, Sawicki GS, Ferris DP (2007) Kinematics and muscle activity of individuals with incomplete spinal cord injury during treadmill stepping with and without manual assistance. *J Neuroeng Rehabil* 4:32. <https://doi.org/10.1186/1743-0003-4-32>
- Dovoedo YH, Chakraborti S (2015) Boxplot-based outlier detection for the location-scale family. *Commun Stat Simul Comput* 44:1492–1513. <https://doi.org/10.1080/03610918.2013.813037>
- Estes S, Zarkou A, Hope JM et al (2021) Combined Transcutaneous spinal stimulation and locomotor training to improve walking function and reduce spasticity in subacute spinal cord injury: a randomized study of clinical feasibility and efficacy. *J Clin Med* 10:1167. <https://doi.org/10.3390/jcm10061167>
- Formento E, Minassian K, Wagner F et al (2018) Electrical spinal cord stimulation must preserve proprioception to enable locomotion in humans with spinal cord injury. *Nat Neurosci* 21:1728–1741. <https://doi.org/10.1038/s41593-018-0262-6>
- Gad P, Gerasimenko Y, Zdunowski S et al (2017) Weight bearing over-ground stepping in an exoskeleton with non-invasive spinal cord neuromodulation after motor complete paraplegia. *Front Neurosci* 11:333. <https://doi.org/10.3389/fnins.2017.00333>
- Gerasimenko Y, Roy RR, Edgerton VR (2008) Epidural stimulation: Comparison of the spinal circuits that generate and control locomotion in rats, cats and humans. *Exp Neurol* 209:417–425. <https://doi.org/10.1016/j.expneurol.2007.07.015>
- Gerasimenko Y, Gorodnichev R, Moshonkina T et al (2015a) Transcutaneous electrical spinal-cord stimulation in humans. *Ann Phys Rehabil Med* 58:225–231. <https://doi.org/10.1016/j.rehab.2015.05.003>
- Gerasimenko Y, Lu DC, Modaber M et al (2015b) Noninvasive reactivation of motor descending control after paralysis. *J Neurotrauma* 32:1968–1980. <https://doi.org/10.1089/neu.2015.4008>
- Gill ML, Grahn PJ, Calvert JS et al (2018) Neuromodulation of lumbosacral spinal networks enables independent stepping after complete paraplegia. *Nat Med* 24:1677–1682. <https://doi.org/10.1038/s41591-018-0175-7>
- Grahn PJ, Lavrov IA, Sayenko DG et al (2017) Enabling task-specific volitional motor functions via spinal cord neuromodulation in a human with paraplegia. *Mayo Clin Proc* 92:544–554. <https://doi.org/10.1016/j.mayocp.2017.02.014>
- Harvey LA (2016) Physiotherapy rehabilitation for people with spinal cord injuries. *J Physiother* 62:4–11. <https://doi.org/10.1016/j.jphys.2015.11.004>
- Hayes SC, James Wilcox CR, Forbes White HS, Vanicek N (2018) The effects of robot assisted gait training on temporal-spatial characteristics of people with spinal cord injuries: a systematic review. *J Spinal Cord Med* 41:529–543. <https://doi.org/10.1080/10790268.2018.1426236>
- Hedges L, v, Pustejovsky JE, Shadish WR, (2013) A standardized mean difference effect size for multiple baseline designs across individuals. *Res Synth Methods* 4:324–341. <https://doi.org/10.1002/jrsm.1086>
- Hofer AS, Schwab ME (2019) Enhancing rehabilitation and functional recovery after brain and spinal cord trauma with electrical neuromodulation. *Curr Opin Neurol* 32:828–835. <https://doi.org/10.1097/WCO.0000000000000750>
- Hofstoetter US, Krenn M, Danner SM et al (2015) Augmentation of voluntary locomotor activity by transcutaneous spinal cord stimulation in motor-incomplete spinal cord-injured individuals. *Artif Organs* 39:E176–E186. <https://doi.org/10.1111/aor.12615>
- Hofstoetter US, Freundl B, Binder H, Minassian K (2018) Spinal cord stimulation as a neuromodulatory intervention for altered motor control following spinal cord injury. *Biosystems and Biorobotics*. Springer, Cham, pp 501–521
- Hornby TG, Zemon DH, Campbell D (2005) Robotic-assisted, body-weight-supported treadmill training in individuals following motor incomplete spinal cord injury. *Phys Ther* 85:52–66
- Hubli M, Dietz V (2013) The physiological basis of neurorehabilitation—locomotor training after spinal cord injury. *J Neuroeng Rehabil* 10:5. <https://doi.org/10.1186/1743-0003-10-5>
- James ND, McMahon SB, Field-Fote EC, Bradbury EJ (2018) Neuromodulation in the restoration of function after spinal cord injury. *Lancet Neurol* 17:905–917. [https://doi.org/10.1016/S1474-4422\(18\)30287-4](https://doi.org/10.1016/S1474-4422(18)30287-4)

- Jankowska E (2017) Spinal control of motor outputs by intrinsic and externally induced electric field potentials. *J Neurophysiol.* <https://doi.org/10.1152/jn.00169.2017>
- Ježerník S, Colombo G, Keller T et al (2003) Robotic orthosis lokomat: a rehabilitation and research tool. *Neuromodulation* 6:108–115. <https://doi.org/10.1046/j.1525-1403.2003.03017.x>
- Koenig A, Omlin X, Bergmann J et al (2011) Controlling patient participation during robot-assisted gait training. *J Neuroeng Rehabil* 8:14. <https://doi.org/10.1186/1743-0003-8-14>
- Loh W-L (1996) On Latin Hypercube Sampling. *Ann Stat* 24:2058–2080
- Luque-Casado A, Rodríguez-Freiría R, Fogelson N et al (2020) An integrative clustering approach to tDCS individual response variability in cognitive performance: beyond a null effect on working memory. *Neuroscience* 443:120–130. <https://doi.org/10.1016/j.neuroscience.2020.07.036>
- Mayr W, Krenn M, Dimitrijevic MR (2016) Epidural and transcutaneous spinal electrical stimulation for restoration of movement after incomplete and complete spinal cord injury. *Curr Opin Neurol* 29:721–726. <https://doi.org/10.1097/WCO.0000000000000382>
- McHugh LV, Miller AA, Leech KA et al (2020) Feasibility and utility of transcutaneous spinal cord stimulation combined with walking-based therapy for people with motor incomplete spinal cord injury. *Spinal Cord Ser Cases* 6:104. <https://doi.org/10.1038/s41394-020-00359-1>
- Megía García A, Serrano-Muñoz D, Taylor J et al (2020) Transcutaneous spinal cord stimulation and motor rehabilitation in spinal cord injury: a systematic review. *Neurorehabil Neural Repair* 34:3–12. <https://doi.org/10.1177/1545968319893298>
- Meyer C, Hofstoetter US, Hubli M et al (2020) Immediate Effects of Transcutaneous Spinal Cord Stimulation on Motor Function in Chronic, Sensorimotor Incomplete Spinal Cord Injury. *J Clin Med.* <https://doi.org/10.3390/jcm9113541>
- Minassian K, Persy I, Rattay F et al (2007) Posterior root-muscle pre-reflexes elicited by transcutaneous stimulation of the human lumbar-sacral cord. *Muscle Nerve* 35:327–336. <https://doi.org/10.1002/mus.20700>
- Minassian K, Hofstoetter U, Tansey K, Mayr W (2012) Neuromodulation of lower limb motor control in restorative neurology. *Clin Neurol Neurosurg* 114:489–497. <https://doi.org/10.1016/j.clineuro.2012.03.013>
- Minassian K, Hofstoetter US, Danner SM et al (2016) Spinal rhythm generation by step-induced feedback and transcutaneous posterior root stimulation in complete spinal cord-injured individuals. *Neurorehabil Neural Repair* 30:233–243. <https://doi.org/10.1177/1545968315591706>
- Mukaka MM (2012) Statistics corner: A guide to appropriate use of correlation coefficient in medical research. *Malawi Med J* 24:69–71
- Murray LM, Knikou M (2019) Transspinal stimulation increases motoneuron output of multiple segments in human spinal cord injury. *PLoS ONE* 14:e0213696. <https://doi.org/10.1371/journal.pone.0213696>
- Musselman KE, Shah M, Zariffa J (2018) Rehabilitation technologies and interventions for individuals with spinal cord injury: translational potential of current trends. *J Neuroeng Rehabil* 15:40. <https://doi.org/10.1186/s12984-018-0386-7>
- Preacher KJ (2001) Calculation for the chi-square test: an interactive calculation tool for chi-square tests of goodness of fit and independence [Computer software]. <http://quantpsy.org/chisq/chisq.htm>. Accessed 13 Dec 2022
- Pulverenti TS, Zaaya M, Grabowski M et al (2021) Neurophysiological changes after paired brain and spinal cord stimulation coupled with locomotor training in human spinal cord injury. *Front Neurol* 12:627975. <https://doi.org/10.3389/fneur.2021.627975>
- Riener R, Lünenburger L, Ježerník S et al (2005) Patient-cooperative strategies for robot-aided treadmill training: first experimental results. *IEEE Trans Neural Syst Rehabil Eng* 13:380–394. <https://doi.org/10.1109/TNSRE.2005.848628>
- Riener R, Lünenburger L, Colombo G (2006) Human-centered robotics applied to gait training and assessment. *J Rehabil Res Dev* 43:679–694
- Rowald A, Komi S, Demesmaeker R et al (2022) Activity-dependent spinal cord neuromodulation rapidly restores trunk and leg motor functions after complete paralysis. *Nat Med* 28:260–271. <https://doi.org/10.1038/s41591-021-01663-5>
- Saraçlı S, Doğan N, Doğan İ (2013) Comparison of hierarchical cluster analysis methods by cophenetic correlation. *J Inequal Appl* 2013:203. <https://doi.org/10.1186/1029-242X-2013-203>
- Sayenko DG, Rath M, Ferguson AR et al (2019) Self-assisted standing enabled by non-invasive spinal stimulation after spinal cord injury. *J Neurotrauma* 36:1435–1450. <https://doi.org/10.1089/neu.2018.5956>
- Schwertman NC, Owens MA, Adnan R (2004) A simple more general boxplot method for identifying outliers. *Comput Stat Data Anal* 47:165–174. <https://doi.org/10.1016/j.csda.2003.10.012>
- Shields MD, Zhang J (2016) The generalization of Latin hypercube sampling. *Reliab Eng Syst Saf* 148:96–108. <https://doi.org/10.1016/j.ress.2015.12.002>
- Smith AC, Knikou M (2016) A review on locomotor training after spinal cord injury: reorganization of spinal neuronal circuits and recovery of motor function. *Neural Plast* 2016:1216258. <https://doi.org/10.1155/2016/1216258>
- Wagner FB, Mignardot JB, le Goff-Mignardot CG et al (2018) Targeted neurotechnology restores walking in humans with spinal cord injury. *Nature* 563:65–93. <https://doi.org/10.1038/s41586-018-0649-2>
- Wernig A, Nanassy A, Müller S (1999) Laufband (treadmill) therapy in incomplete paraplegia and tetraplegia. *J Neurotrauma* 16:719–726. <https://doi.org/10.1089/neu.1999.16.719>
- Winchester P, McColl R, Querry R et al (2005) Changes in supraspinal activation patterns following robotic locomotor therapy in motor-incomplete spinal cord injury. *Neurorehabil Neural Repair* 19:313–324. <https://doi.org/10.1177/1545968305281515>
- Winchester P, Smith P, Foreman N et al (2009) A prediction model for determining over ground walking speed after locomotor training in persons with motor incomplete spinal cord injury. *J Spinal Cord Med* 32:63–71. <https://doi.org/10.1080/10790268.2009.11760754>
- Wirz M, Zemon DH, Rupp R et al (2005) Effectiveness of automated locomotor training in patients with chronic incomplete spinal cord injury: a multicenter trial. *Arch Phys Med Rehabil* 86:672–680. <https://doi.org/10.1016/j.apmr.2004.08.004>
- Zaaya M, Pulverenti TS, Knikou M (2021) Transspinal stimulation and step training alter function of spinal networks in complete spinal cord injury. *Spinal Cord Ser Cases* 7:55. <https://doi.org/10.1038/s41394-021-00421-6>

Publisher's Note Springer Nature remains neutral with regard to jurisdictional claims in published maps and institutional affiliations.

Springer Nature or its licensor (e.g. a society or other partner) holds exclusive rights to this article under a publishing agreement with the author(s) or other rightsholder(s); author self-archiving of the accepted manuscript version of this article is solely governed by the terms of such publishing agreement and applicable law.

Authors and Affiliations

Matthias J. Krenn^{1,2,3}  · Jason M. White^{4,5}  · Dobrivoje S. Stokic²  · Keith E. Tansey^{1,2,6} 

Jason M. White
jwhite60@gatech.edu

Dobrivoje S. Stokic
dstokic@mmrcrehab.org

Keith E. Tansey
ktansey@mmrcrehab.org

¹ Department of Neurosurgery, University of Mississippi Medical Center, 2500 N State St, Jackson, MS 39216, USA

² Center for Neuroscience and Neurological Recovery, Methodist Rehabilitation Center, 1350 E Woodrow Wilson Ave, Jackson, MS 39216, USA

³ Paralysis Center, Department of Neurosurgery, Massachusetts General Hospital, 15 Parkman St, Wang 745, Boston, MA 02114, USA

⁴ Department of Biomedical Engineering, Georgia Institute of Technology, 313 First Drive, Atlanta, GA 30332, USA

⁵ Department of Physiology, Emory University, 12 Executive Park Dr NE, Atlanta, GA 30322, USA

⁶ Spinal Cord Injury Medicine and Research Services, VA Medical Center, 1500 E Woodrow Wilson Ave, Jackson, MS 39216, USA